

Experimental Assessment of Harmonic Contributions Using a Ternary Pulse Sequence

Evgeniia Bulycheva¹, Sergey Yanchenko¹

Abstract: Harmonic contributions of utility and customer may feature significant variations due to network switchings and changing operational modes. In order to correctly define the impacts on the grid voltage distortion the frequency dependent impedance characteristic of the studied network should be accurately measured in the real-time mode. This condition can be fulfilled by designing a stimuli generator measuring the grid impedance as a response to injected interference and producing time-frequency plots of harmonic contributions during considered time interval. In this paper a prototype of a stimuli generator based on programmable voltage source inverter is developed and tested. The use of ternary pulse sequence allows fast wide-band impedance measurements that meet the requirements of real-time assessment of harmonic contributions. The accuracy of respective analysis involving impedance determination and calculation of harmonic contributions is validated experimentally using reference characteristics of laboratory test set-up with varying grid impedance.

Keywords: Harmonic identification, Harmonic contribution, Impedance measurement, Non-linear load, Power quality, Ternary pulse sequence.

1 Introduction

The sophistication of production processes, implementation of new types of energy efficient industrial equipment and control techniques bring about new challenges for power quality management. In fact, continuous changes of equipment operating modes, multiple switchings of network topologies complicate deterministic design-based assessment of power quality indices thus favoring the use of more straightforward measurement based approaches. In this way the introduction of measurement systems allowing continuous power quality monitoring may not only provide the primary control of the indices versus the standard's limits but also allow more complex online data analysis, e.g. real-time harmonic identification.

¹Department of Power Supply of Industrial Enterprises and Electrotechnologies, Moscow Power Engineering Institute, Krasnokazarmennaya str. 14, 111250, Moscow, Russia;
E-mails: BulychevaYA@mpei.ru; yanchenko_sa@mail.ru

Previously developed method for the determination of customer harmonic contributions [1] provides real-time information on the grid impact of selected nonlinear loads. The use of short-time stimuli allows to define the frequency-dependent grid impedance in the range of up to 2 kHz with the time step of 80 ms resulting in high-resolution profile of harmonic contribution for multiple harmonic orders. This method for real-time harmonic identification was implemented in MATLAB/Simulink and validated theoretically for the pool of multiple simulations with randomly varying grid parameters [1]. Its main limitation however, consists in the need for a stimuli generator, a programmable voltage source inverter controlled via a digital signal processing (DSP) chip. The purpose of the generator is to inject a specified measurement stimuli into considered network, thus allowing determination of corresponding frequency-dependent impedance and, hence, harmonic contributions. Challenges with the practical implementation of the stimuli generator impeded the experimental verification of the proposed approach in [1]. Therefore, the present paper aims to compensate for this shortcoming by describing a built prototype of a stimuli generator and demonstrating its use within the proposed method for real-time harmonic identification.

The paper is organized as follows. Section 2 discusses the theoretical background of the developed method. General description of the stimuli generator is provided in Section 3. Experimental verification of the developed generator is described in Section 4. Section 5 presents harmonic impedance assessment in laboratory conditions for various generator parameters. Experimental harmonic contribution assessment is conducted in Section 6. Finally, current results of the research are discussed.

2 Developed Method for Calculation of Harmonic Contributions

A need for correct assessment of the influence of nonlinear loads on the grid voltage distortion has led to the emergence of numerous methods for calculation of harmonic contributions [2 – 3]. Nevertheless, generally they share a common approach for the assessment of harmonic contributions that is based on the grid representation of Fig. 1.

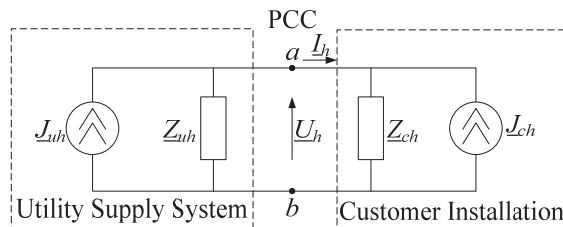


Fig. 1 – Equivalent grid representation at particular harmonic frequency.

Harmonic voltage U_h at the point of common coupling (PCC) is formed by the joint impacts of utility and customer that are modeled as current harmonic sources J_{uh} and J_{ch} in parallel with respective linear harmonic impedances Z_{uh} and Z_{ch} (Fig.1), where h is harmonic order up to 40:

$$\underline{U}_h = \underline{U}_{uh} + \underline{U}_{ch}. \quad (1)$$

Here \underline{U}_{uh} and \underline{U}_{ch} are the utility and customer contributions to voltage distortion at PCC at particular harmonic frequency that may be determined using harmonic voltage \underline{U}_h and load current \underline{I}_h in accordance with:

$$\underline{U}_{uh} = (\underline{U}_h - \underline{Z}_{uh} \underline{I}_h) \frac{\underline{Z}_{ch}}{\underline{Z}_{uh} + \underline{Z}_{ch}}, \quad (2)$$

$$\underline{U}_{ch} = (\underline{U}_h + \underline{Z}_{ch} \underline{I}_h) \frac{\underline{Z}_{uh}}{\underline{Z}_{uh} + \underline{Z}_{ch}}. \quad (3)$$

As \underline{U}_h and \underline{I}_h are derived from the measurement data, it follows from (2) and (3), that accuracy of harmonic contribution assessment depends mainly on the accuracy of determined harmonic impedances Z_{ch} and Z_{uh} .

Obtaining reliable information about the utility impedance is significantly complicated by the multicomponent nature of modern network, the lack of complete information about the structure and connected loads, and the random nature of power consumption. In addition, a large number of nonlinear loads with a capacitive characteristic of the input impedance in modern network collectively create conditions for the occurrence of resonances. This is significantly complicates the calculation of harmonic contribution.

In this paper, frequency-dependent impedances are estimated using experimental active approach, i.e., by applying measured response of the studied network to the intentionally constructed stimuli [4]. Thus, uncertainties of theoretical calculation using rated data of network equipment are excluded and real-time impedance value is provided.

Following this active measurement approach, previously developed method for harmonic identification [1] uses a ternary pulse sequence as injected stimuli in order to determine frequency-dependent impedance characteristics. Ternary pulse sequence features multiple advantages over typically adopted stimuli signals (e.g. sinusoidal frequency sweep [5 – 7] or network switching transients [8 – 11]) that make it perfectly adopted for online impedance evaluation [12]:

- wide uniform spectrum assures sufficient signal-to-noise ratio and, hence, accuracy over entire frequency range of interest;
- short length allows multiple injections and, hence, high time resolution of impedance calculation;
- low magnitude guarantees negligible impact on the operation of sensitive network equipment.

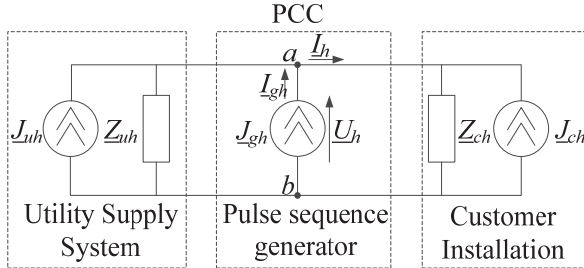


Fig. 2 – Equivalent network representation with the pulse sequence generator.

With the ternary pulse sequence injected by the stimuli generator (Fig. 2) signals of voltage $u(t)$, load current $i(t)$ and generator current $i_g(t)$ at the PCC are measured and decomposed with the short-term Fourier transform into time-spectral components $U_h(t)$, $I_h(t)$, $I_{gh}(t)$. Customer and utility harmonic impedances Z_{ch} and Z_{uh} are determined under the assumption of their linear nature, i.e. that impedance values at particular frequency may be determined by the ratio of respective voltage and current harmonics:

$$\underline{Z}_{ch} = \frac{U_h}{I_h}, \quad (4)$$

$$\underline{Z}_{uh} = \frac{U_h}{(I_h + I_{gh})}, \quad (5)$$

where U_h is the harmonic voltage at the PCC, I_h is the load current, I_{gh} is the generator current.

These are further used to calculate time-varying network $Z_{uh}(t)$ and customer $Z_{ch}(t)$ impedances at interharmonic frequencies thus avoiding the impact of inherent nonlinearities of the network [4]:

$$\underline{Z}_h(t) = \frac{\underline{Z}_{h-1}(t) + \underline{Z}_{h+1}(t)}{2}. \quad (6)$$

Impedance values at particular harmonic frequencies are inserted in (2), (3) and corresponding harmonic contributions are determined.

If there are several harmonic sources in the network, the proposed method is applied separately for each nonlinear load. That is, one harmonic source is allocated as a customer, and the rest of the network is considered as a system.

The theoretical verification of the proposed method for harmonic identification was produced in Matlab/Simulink in [1]. In this paper for the experimental verification of the method a prototype of a pulse sequence generator is designed and tested by analyzing the accuracy of the impedance estimation.

3 General Description of the Ternary Pulse Sequence Generator

Basic structure of a ternary pulse sequence generator is shown in Fig. 3. The ternary pulse sequence generator parameters are presented in the **Table 1**.

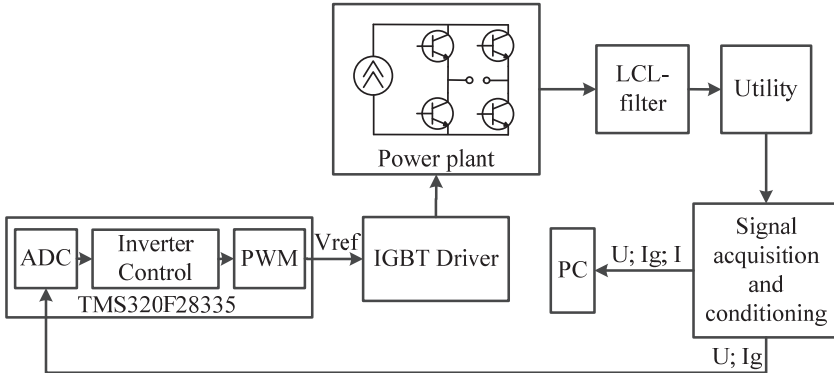


Fig. 3 – Basic structure of a ternary pulse sequence generator.

Table 1
The Ternary Pulse Sequence Generator Parameters.

V_{DC} [V]	V_{AC} [V]	PWM frequency [Hz]	rated power [W]	Length of the pulse sequence
380	220	20 000	200	1009-bit

Inherently, it corresponds to a standard single-phase voltage source inverter with the output current programmed by the DSP-chip that is used to set the parameters of the measurement stimuli. A power plant of the generator features typical structure [13] including a DC-link based on a 380 V DC power supply, an IGBT-bridge and an input LCL-filter. IGBT-bridge receives control signals through drivers, which provide power amplification of control signals and galvanic isolation between individual units of the device. Data acquisition system includes grid voltage and current sensors and signal conditioning circuits in order to comply with the input requirements of the ADC. Acquired signals are fed to the DSP evaluation board with TMS320F28335 controller that is used to implement the control algorithm of the pulse sequence generator. Hereafter, a more detailed description of particular blocks of the designed generator prototype is provided.

Control algorithm of the pulse sequence generator was first developed as a Simulink-based model (Fig. 4) and then automatically converted into the C-code implementable into the DSP controller. The model itself consists of the several levels. The highest level (Fig. 4) contains the specified parameters for the interrupt routine of the DSP-controller, blocks assuring the soft-start of inverter and the input of the ternary pulse sequence.

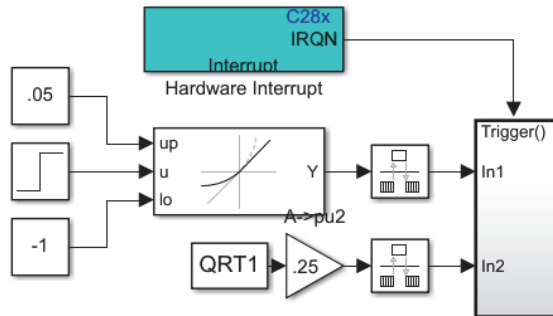


Fig. 4 – The highest level of the generator control model.

The medium level of the model (Fig. 5) represents a triggered subsystem that is executed during the hardware interrupt and includes inverter control and peripherals of the DSP controller: ADC and PWM modules. The ADC conversion is started by the interrupt event at the beginning and at the end of the PWM period.

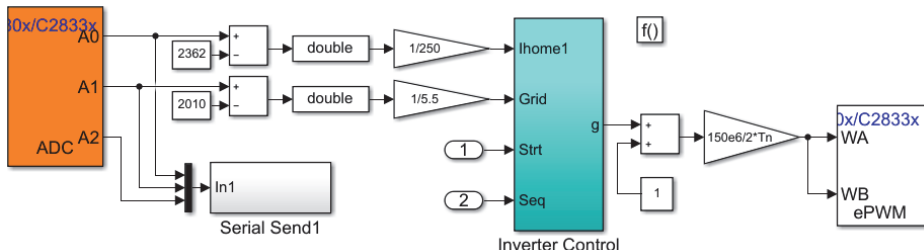


Fig. 5 – Medium level of the generator control model.

The measured data are processed by the inverter control block in order to produce an input signal for the PWM block. Furthermore, data logging required for subsequent calculation of impedance and harmonic contributions is accomplished by the Serial Send subsystem. It converts the ADC output signals and sends them via serial connection interface to an additional model (Fig. 6) utilized for storing the measurement data in PC [14].

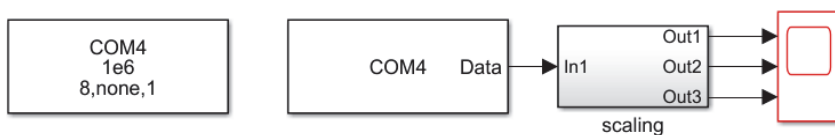


Fig. 6 – Additional model for logging of measurement data.

Experimental Assessment of Harmonic Contributions Using a Ternary Pulse Sequence

The lowest level of the model represents the structure of inverter control system (Fig. 7) and consists of a phase locked loop (PLL) and a PI-based current control loop with the grid voltage feed-forward [15]. The generator output current is regulated in order to match with the reference signal that is composed by a normalized grid sinusoid and a ternary pulse sequence.

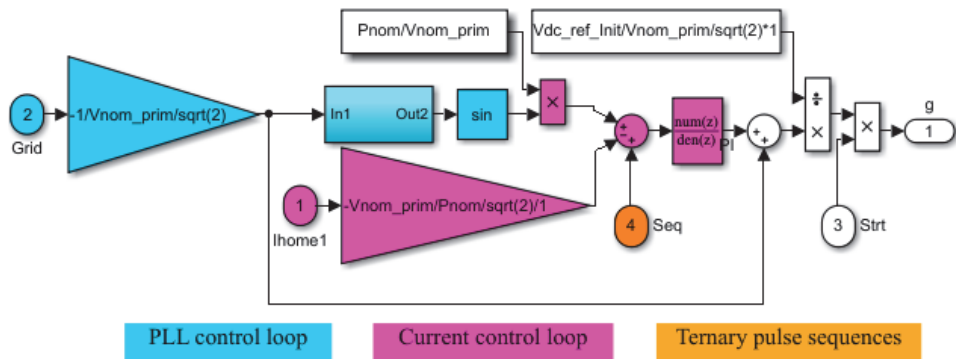


Fig. 7 – Inverter control subsystem.

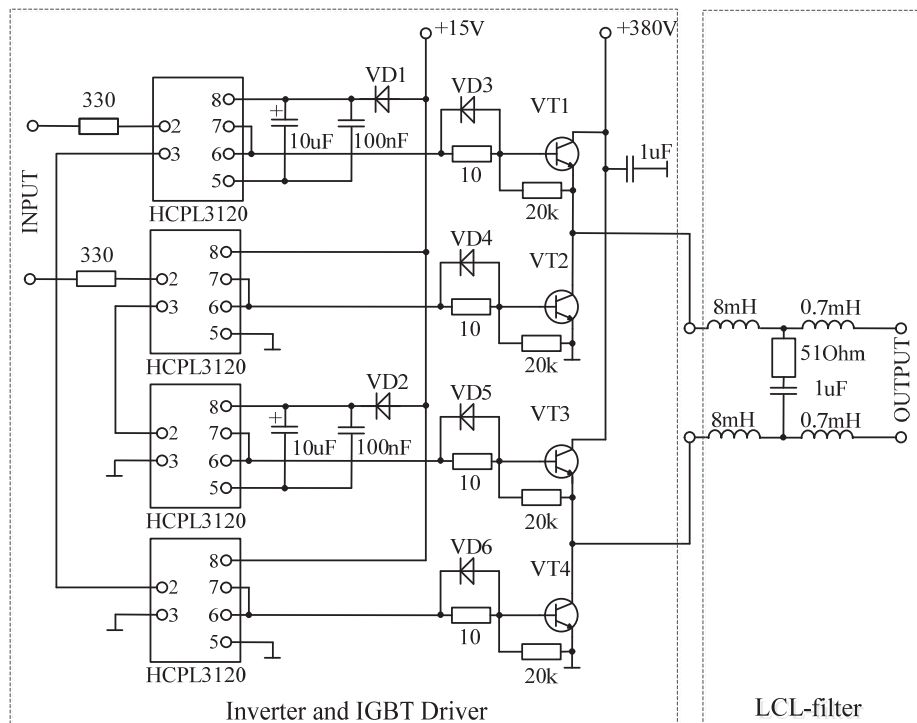


Fig. 8 – Power plant with IGBT-driver, inverter and LCL-filter.

In this way, the implementation of the described three-level control model in the DSP controller allows to produce PWM switching signals that ensure the required harmonic content of the stimuli at the output of the pulse sequence generator.

The electric circuit of the power plant, including IGBT-driver, single-phase bridge inverter and input LCL-filter is presented in Fig. 8. Inverter IGBT-switches are supplied with the PWM control signals from the DSP controller through the IGBT optrons that provide signal amplification and galvanic isolation of the controller circuitry [16]. High-frequency switching distortion of inverter output current is attenuated by the LCL-filter.

Electric circuit of the signal acquisition and conditioning board is presented in Fig. 9 and consists of voltage and current sensors and corresponding signal processing elements [17] ensuring the compliance with the ADC. For example, the output of the voltage sensor is scaled and shifted by the operational amplifier producing a unipolar scaled equivalent of the grid voltage that is suitable for further use in the control algorithm.

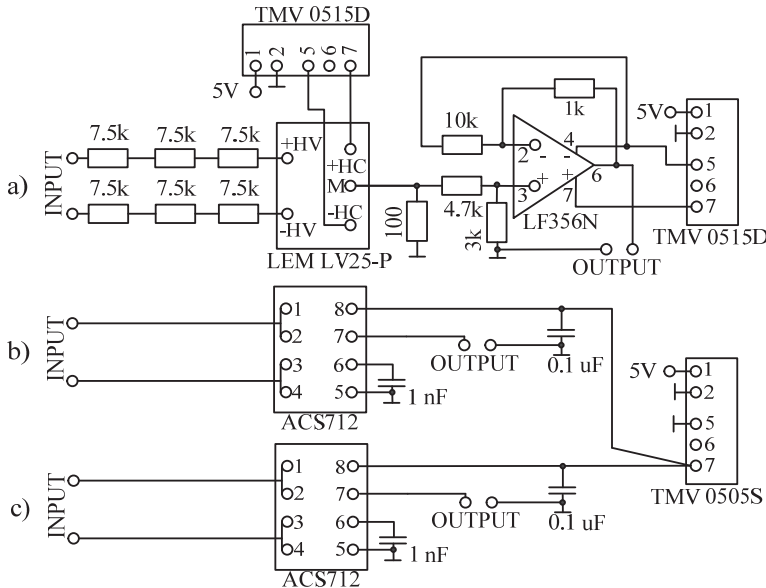


Fig. 9 – Signal acquisition and conditioning: (a) AC voltage sensor; (b) current sensor at the generator's output; (c) current sensor of nonlinear load.

Fig. 10 shows a general view of the designed ternary pulse sequence generator consisting of previously described parts: 1 – LCL-filter, 2 – power plant, 3 – DSP-controller, 4 – signal acquisition and conditioning board.

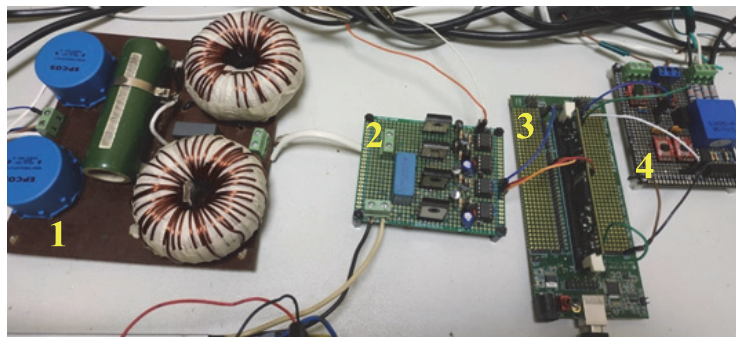


Fig. 10 – Ternary pulse sequence generator (1 – LCL-filter, 2 – power plant, 3 – DSP-controller, 4 – signal acquisition and conditioning board).

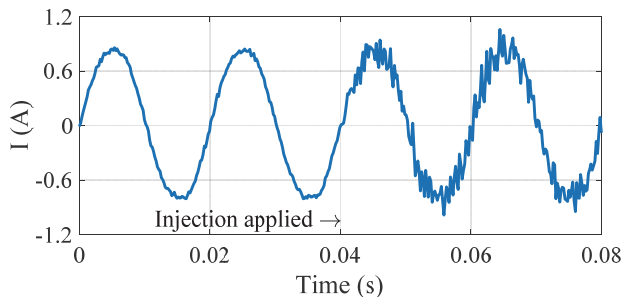


Fig. 11 – Measured current responses during the injection of the ternary pulse sequence.

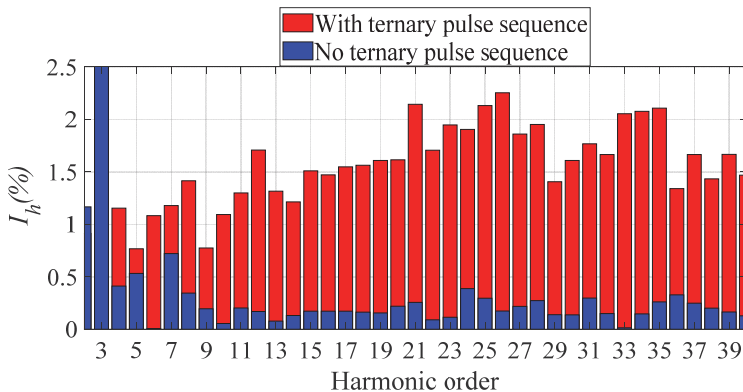


Fig. 12 – Current spectrum before and after the injection of the ternary pulse sequence.

Fig. 11 demonstrates the output current of the generator at the time of the injection of the ternary pulse sequence. The spectrum of this current with and

without interference is shown in Fig. 12. Produced ternary pulse sequence features wide sufficiently uniform spectrum with relatively low harmonic magnitudes.

4 Testing of the Developed Pulse Sequence Generator

In order to evaluate the effectiveness of the developed stimuli generator a grid impedance test-bed was constructed in accordance with Fig. 13. The use of capacitive and inductive elements along with the switches allowed to produce switchings between multiple impedance characteristics including resonant.

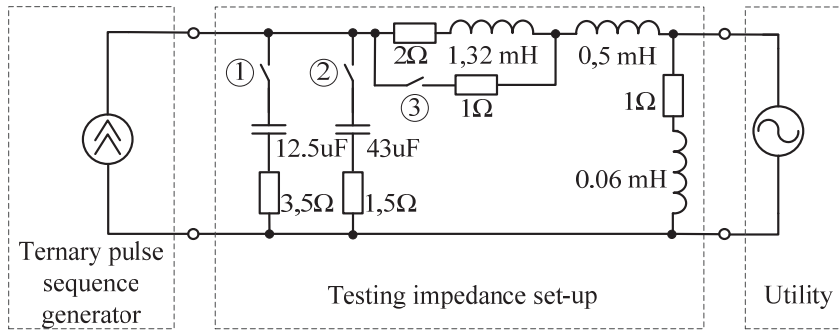


Fig. 13 – A circuit of grid impedance test-bed.

Testing activities implied connection of the generator, that was continuously injecting stimuli, to the grid impedance test-bed and measurement of the system response while varying the states of the switches (**Table 2**) and thus changing impedance characteristics.

Table 2
Switching sequence of the grid impedance test-bed.

INTERVAL	TIME [s]	SWITCH 1	SWITCH 2	SWITCH 3
1	0-5.5		open	
2	5.5-12.2	closed	open	open
3	12.2-16	open	open	closed

The resulting data were used to build time-frequency impedance plots (Fig. 14) showing switchings between frequency characteristic at particular time instants. Measured impedances feature distinct characteristics, e.g. resonant or inductive, that are correctly reproduced with the help of pulse sequence generator.

Additionally, Fig. 15 presents a comparison of measured frequency-dependent impedances (blue lines) with theoretical characteristics (red lines) calculated for particular configurations of the test-bed using known values of circuit elements. The matching is generally good over entire frequency range.

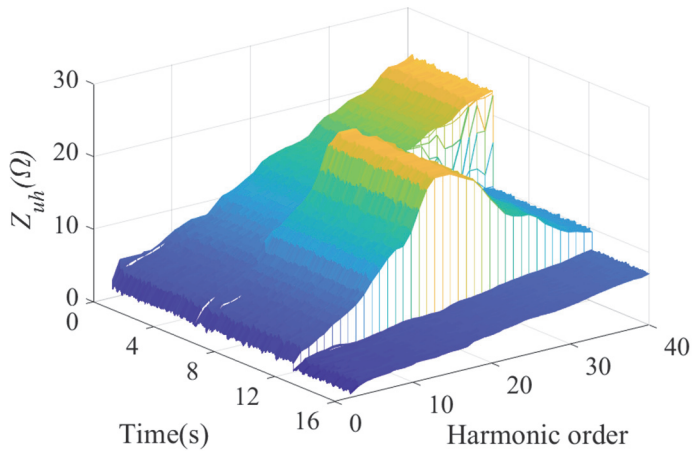


Fig. 14 – Measured time-frequency impedance of the grid test-bed.

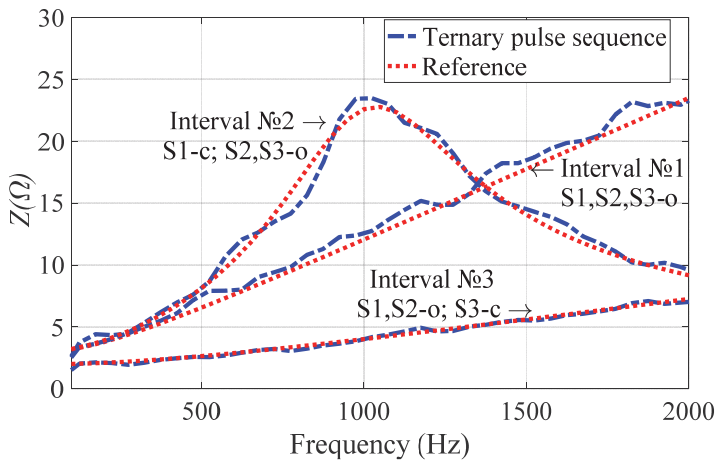


Fig. 15 – Comparison of measured frequency-dependent impedance (dash lines) with theoretical characteristics (square dot lines) ('o' – 'open', 'c' – 'closed').

5 Optimizing Generator Parameters for Better Accuracy of Impedance Estimation

This section analyzes the impact of the generator parameters on the accuracy of experimentally determined harmonic impedance. Resonant configuration of the grid impedance test-bed (Interval 2 in **Table 2**, Fig. 15) was selected for the error assessment of measured impedance in respect to the reference under varying parameters of the pulse sequence generator: proportional gain of the PI-controller and magnitude of the stimuli. For each case, multiple parameter values from

typical variation ranges were implemented in the generator control system and corresponding frequency-dependent impedance was measured.

Hereafter, the bar plots (Fig. 16) that depict relative errors of harmonic magnitudes in the frequency range of up to 2 kHz, are presented for some characteristic values of each parameter. In Fig. 16a the variation of proportional gain of PI-controller is presented, in Fig. 16b the variation of the stimuli magnitude. All characteristics feature similar behavior with the highest errors observed for the low order harmonics and almost perfect matching in the higher frequency range. These inaccuracies result from the presence of inherent nonlinearities revealing themselves as low order harmonics of the grid voltage and generator output current. These harmonics superimpose with the measured system response and distort the results [12].

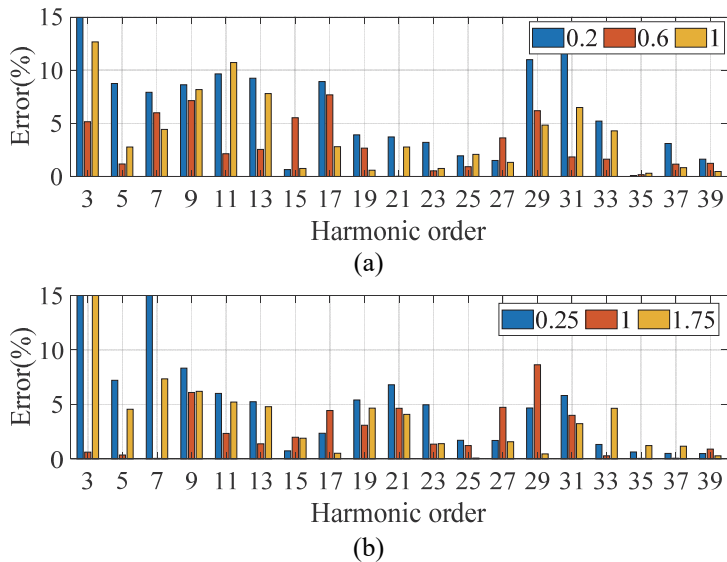


Fig. 16 – Relative errors of harmonic magnitudes: (a) the variation of proportional gain of PI-controller; (b) the variation of the stimuli magnitude.

The integral estimation of the accuracy in considered frequency range was produced for multiple parameter values by calculating the root mean square error (RMSE) in accordance with:

$$\rho = \frac{\sum_{i=1}^n (x_i - \bar{x})(y_i - \bar{y})}{\sqrt{\sum_{i=1}^n (x_i - \bar{x})^2 \sum_{i=1}^n (y_i - \bar{y})^2}}, \quad (7)$$

where x and y are the calculated and reference values; σ_x and σ_y are the variances of x and y ; σ_{xy} is the covariance between x and y ; \bar{x} and \bar{y} are the mean values of x and y .

The resulting plots of RMSE variation are shown in Fig. 17. The increase of the proportional gain of PI-controller generally reduces the error of the estimated impedance (Fig. 17a) as the capability of the generator to accurately reproduce the specified ternary pulse sequence is improved. Higher magnitude of the ternary pulse sequence predictably provides better accuracy of impedance measurement (Fig. 17b) as the signal-to-noise ratio of the measured data increases.

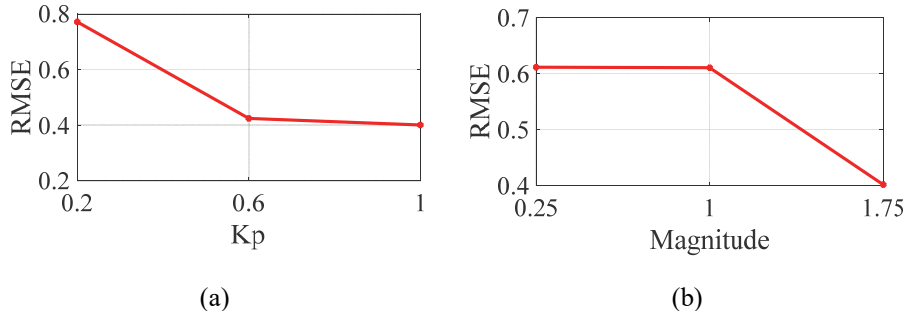


Fig. 17 – RMSE for different values K_p : (a) and for different magnitude of injection (b).

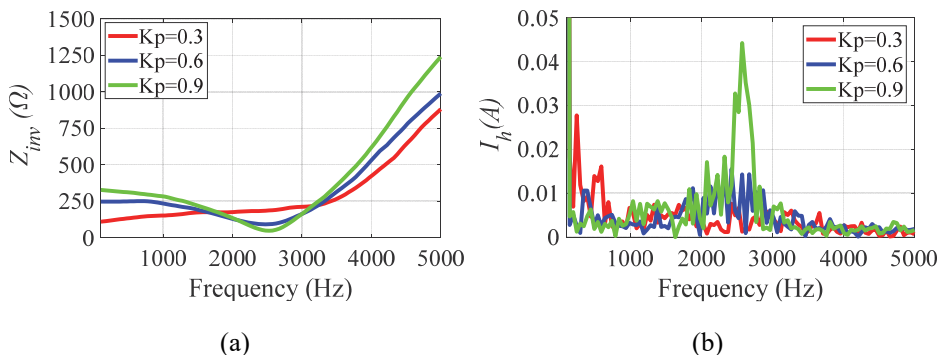


Fig. 18 – Impact of proportional gain on performance of the stimuli generator: (a) input impedance characteristics; (b) spectra of the output current.

The impact of proportional gain of PI-controller on the accuracy of impedance estimation was further studied by producing input impedance characteristics of the pulse sequence generator. Impedance plots corresponding to particular values of proportional gain (Fig. 18a) were produced by the frequency sweep method [4] in the range of up to 5 kHz. It follows from the figure that unreasonable increase of the gain results in a dip of impedance characteristic

at 2.5 kHz representing arisen instability [18]. This gives rise to additional harmonics appearing in the spectrum of the output current (Fig. 18b) that distort the measured data of impedance estimation. Generally, selection of appropriate proportional gain value represents a tradeoff between sufficient accuracy of harmonic identification and significant operation stability of the pulse sequence generator.

Conducted parameter optimization analysis reveals that generally optimal magnitude and length of injected ternary pulse sequence are selected as a trade off between the signal strength and allowed interference limit. The former affects the accuracy of impedance determination while the latter preserves normal operation of the grid under study. Thus for stiff grids with high short circuit capacity higher magnitude of the stimuli is required while weaker grids may be analyzed with low energy stimuli.

6 Harmonic Contribution Assessment Within the Developed Method

The analysis presented in the previous section allowed to optimize parameter values of the generator for more accurate impedance estimation and experimentally implement the developed method for assessment of harmonic contributions [1]. To this end, the effectiveness of the method is verified in laboratory conditions using a specially designed test set-up shown in Fig. 19.

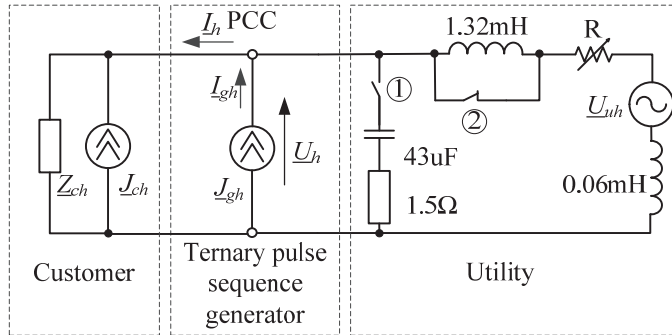


Fig. 19 – Laboratory set-up for testing of the developed method for harmonic identification.

The set-up consists of a utility model featuring voltage supply with inherent harmonic distortion and varying frequency-dependent impedance; a customer represented by nonlinear load; and a ternary pulse sequence generator. Adopted switching sequence of the grid impedance is shown in **Table 3**.

Harmonic spectra of the grid voltage, customer and generator currents is presented in Fig. 20 showing significant impact of customer operation on the

resulting levels of the 3rd and the 5th voltage harmonics. Hereafter customer contribution to the levels of these harmonics is determined using developed method.

Table 3
Switching sequence of the grid impedance.

Interval №	TIME [s]	SWITCH 1	SWITCH 2	R,Ω
1	0-0.7	open	closed	4.6
2	0.7-1.4	closed	closed	4.6
3	1.4-2.1	closed	open	1.3
4	2.1-2.8	open	closed	2.65

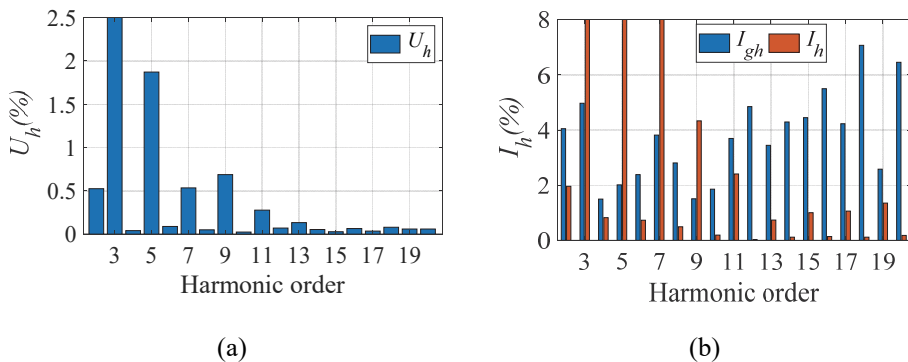


Fig. 20 – Harmonic spectra of the grid voltage (a), generator and customer currents (b).

Multiple injections of ternary pulse sequences with total duration corresponding to considered time interval (**Table 3**) are generated at the PCC using the developed generator. With the measurements of the frequency response to generated stimuli the time-frequency impedance characteristic of the utility can be determined during entire time period. Respective characteristic is presented in Fig. 21 with the reversed frequency axis for better visibility.

A comparison of frequency-dependent impedances at particular time instants (blue lines) with theoretically calculated characteristics (red lines) is shown in Fig. 22 justifying sufficient accuracy of the measured impedance.

Assuming that customer features much higher impedance than the utility, equations (2) and (3) for harmonic contributions can be simplified by neglecting \underline{Z}_{ch} :

$$\underline{U}_{uh} = \lim_{\underline{Z}_{ch} \gg \underline{Z}_{uh}} \frac{(\underline{U}_h - \underline{Z}_{uh} \underline{I}_h) \cdot \underline{Z}_{ch}}{\underline{Z}_{uh} + \underline{Z}_{ch}} = \underline{U}_h - \underline{Z}_{uh} \underline{I}_h, \quad (8)$$

$$\underline{U}_{ch} = \lim_{\underline{Z}_{ch} \ll \underline{Z}_{uh}} \frac{(\underline{U}_h + \underline{Z}_{ch} \underline{I}_h) \cdot \underline{Z}_{uh}}{\underline{Z}_{uh} + \underline{Z}_{ch}} = \underline{Z}_{uh} \underline{I}_h. \quad (9)$$

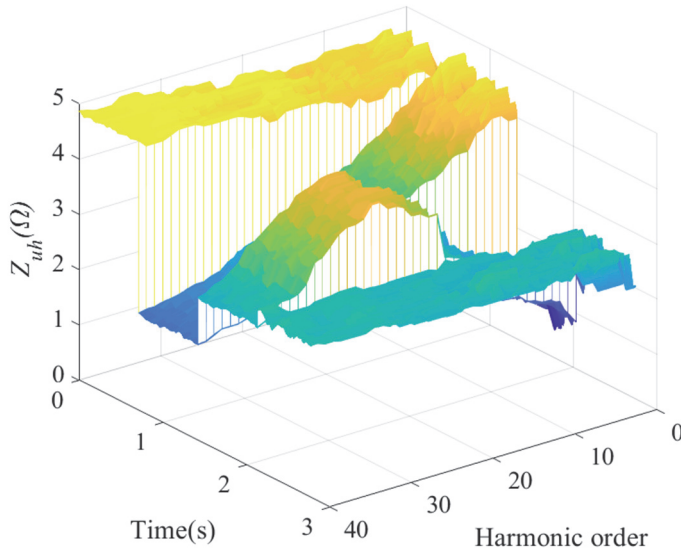


Fig. 21 – Time-frequency impedance of the utility.

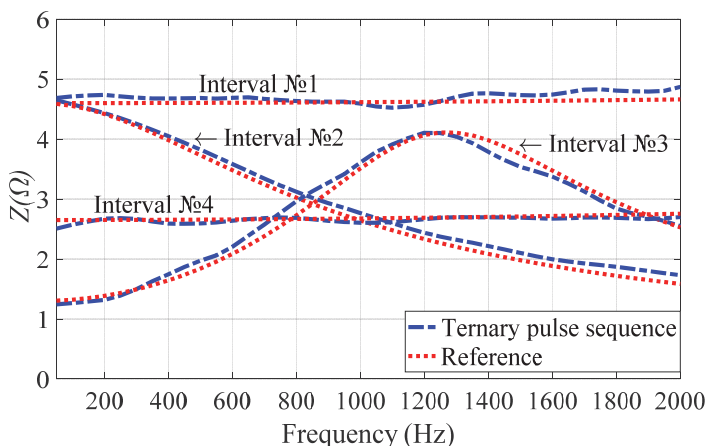


Fig. 22 – Comparison of impedance characteristics measured with the ternary pulse sequence (dash lines) and calculated theoretically based on the circuit parameter values (square dot lines).

Defined impedance values at the 3rd and the 5th harmonics can be used along with measured time varying voltage and current harmonics to (8) and (9) in order to obtain time-varying harmonic contributions of the customer and utility. Corresponding results depicting customer and utility contributions, obtained by the proposed method are presented as 3d bar plots (blue and yellow histograms) in Fig. 23 along with the reference contributions (deep blue and green histograms) for clearer comparison. It follows from the figures, that the developed method accurately determines varying harmonic contributions in accordance with the reference plots.

Time characteristics of the customer contribution at considered harmonics (Fig. 23a) generally follow the variation of impedance at corresponding frequencies. During the first 2 intervals (0 – 1.4 s, **Table 3**) grid impedance value is high (Fig. 22) resulting in significant harmonic voltage drop and, hence, impact of the customer on voltage distortion at PCC. Conversely, the 3rd interval (1.4 – 2.1 s, **Table 3**) features reduced impedance values at the 3rd and the 5th harmonic frequencies leading to a lower harmonic voltage drop and less prominent impact of the customer on voltage distortion at PCC.

Unlike that of the customer, harmonic contribution of the utility (Fig. 23b) does not feature any significant variation and represents distortion levels inherently present in the grid.

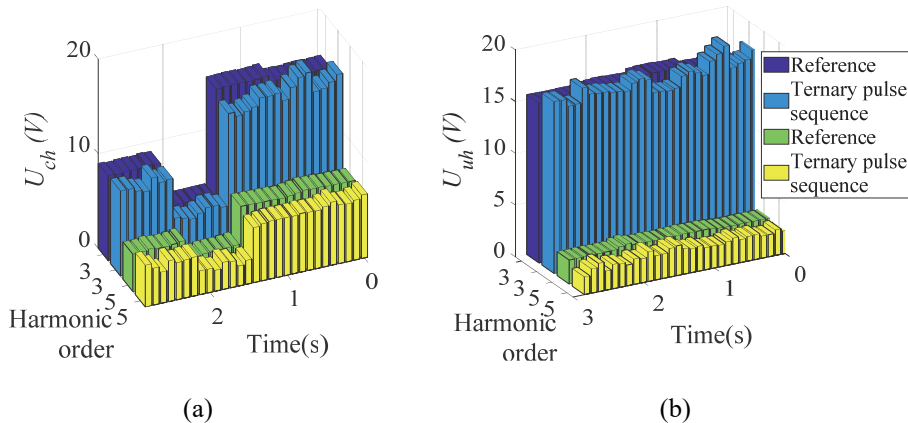


Fig. 23 – Comparison of the reference and measured time-varying harmonic contributions of customer (a) and utility (b) for the 3rd and the 5th harmonics.

7 Conclusion

In this paper, the prototype of the ternary pulse sequence generator is designed and utilized in experimental verification of the recently proposed method for real-time assessment of harmonic contributions. The accuracy of impedance measurement provided by generator is analyzed for typical variation ranges of the control system parameters. Optimized parameter values are further implemented in the generator control system during experimental determination of harmonic contributions for the case of nonlinear load connected to varying grid impedance. Good matching of calculated harmonic contributions with reference characteristics for both customer and utility justifies the applicability of the developed method for the analysis of varying harmonic impacts.

At its current state proposed method of real-time harmonic identification is limited by its single-phase low voltage properties. Introducing a capability to define harmonic contributions for three phase medium voltage networks is seen as a logical extension of the method's functionality and will be considered in the future research.

8 Acknowledgments

The reported study was funded by RFBR, project number 19-38-90264.

9 References

- [1] E.A. Bulycheva, S.A. Yanchenko: Real-Time Harmonic Identification Under Varying Grid Conditions, Serbian Journal of Electrical Engineering, Vol. 18, No.1, February 2021, pp. 29 –48.
- [2] F. Safargholi, K. Malekian, W. Schufft: On the Dominant Harmonic Source Identification - Part I: Review of Methods, IEEE Transactions on Power Delivery, Vol. 33, No. 3, June 2018, pp. 1268–1277.
- [3] T. Zang, Z. He, Y. Wang, L. Fu, Z. Peng, Q. Qian: A Piecewise Bound Constrained Optimization for Harmonic Responsibilities Assessment under Utility Harmonic Impedance Changes, Energies, Vol. 10, No. 7, July 2017, pp. 1–20.
- [4] A. Robert, T. Deflandre et al. (CIGRE/CIRED Working Group CC02): Guide for Assessing the Network Harmonic Impedance, Electra, No. 167, August 1996, pp. 97–131.
- [5] F. Zavoda: Measurement of the Harmonic Impedance of LV Distribution Supply System (120/240V), Proceedings of the 19th International Conference on Electricity Distribution (CIRED), Vienna, Austria, May 2007, pp. 1–4.
- [6] J. Xie, Y.X. Feng, N. Krap: Network Impedance Measurement for Three-Phase High-Voltage Power Systems, Proceedings of the Asia-Pacific Power and Energy Engineering Conference (APPEEC), Chengdu, China, March 2010, pp. 1–5.
- [7] D. Roggo, L. Merendaz, D. Furrer: On-line 2 to 150 kHz Grid Impedance Meter, Proceedings of the 22nd International Conference on Electricity Distribution (CIRED), Stockholm, Sweden, June 2013, pp. 1–4.
- [8] M. Jordan, H. Langkowski, T. Do Thanh, D. Schulz: Frequency Dependent Grid-Impedance Determination with Pulse-Width-Modulation-Signals, Proceedings of the 7th International

Experimental Assessment of Harmonic Contributions Using a Ternary Pulse Sequence

Conference-Workshop Compatibility and Power Electronics (CPE), Tallinn, Estonia, June 2011, pp. 131–136.

- [9] M. Sumner, B. Palethorpe, D.W.P. Thomas, P. Zanchetta, M.C. Di Piazza: A Technique for Power Supply Harmonic Impedance Estimation Using a Controlled Voltage Disturbance, IEEE Transactions on Power Electronics, Vol. 17, No. 2, March 2002, pp. 207–215.
- [10] R. Stiegler, J. Meyer, P. Schegner, D. Chakravorty: Measurement of Network Harmonic Impedance in Presence of Electronic Equipment, Proceedings of the IEEE International Workshop on Applied Measurements for Power Systems (AMPS), Aachen, Germany, September 2015, pp. 49–54.
- [11] W. Wang, E.E. Nino, W. Xu: Harmonic Impedance Measurement Using a Thyristor-Controlled Short Circuit, IET Generation, Transmission & Distribution, Vol. 1, No. 5, September 2007, pp. 707–713.
- [12] T. Roinila, T. Messo: Online Grid-Impedance Measurement Using Ternary-Sequence Injection, IEEE Transactions on Industry Applications, Vol. 54, No. 5, September 2018, pp. 5097–5103.
- [13] Design Guide: TIDM-HV-1PH-DCAC, Grid Connected Inverter Reference Design, User Manual, Texas Instruments, TIDUB21C – November 2015. – Revised May 2019.
- [14] Antonin: DC/DC Buck Converter Example, MATLAB Central File Exchange, Retrieved April 22, 2021, Available at:
<https://www.mathworks.com/matlabcentral/fileexchange/61420-dc-dc-buck-converter-example>
- [15] F. Blaabjerg, R. Teodorescu, M. Liserre, A.V. Timbus: Overview of Control and Grid Synchronization for Distributed Power Generation Systems, IEEE Transactions on Industrial Electronics, Vol. 53, No. 5, October 2006, pp. 1398–1409.
- [16] HCPL3120/J312, HCNW3120, 2.5 Amp Output Current IGBT Gate Drive Optocoupler, Datasheet, Avago Technologies, Available at:
<http://www.farnell.com/datasheets/2111191.pdf>
- [17] Step-by-Step Design of a Voltage Sensing PCB, Available at:
<https://www.switchcraft.org/project-blog/2016/12/11/designing-a-voltage-sensing-pcb>
- [18] J. Dannehl, C. Wessels, F.W. Fuchs: Limitations of Voltage-Oriented PI Current Control of Grid-Connected PWM Rectifiers with LCL Filters, IEEE Transactions on Industrial Electronics, Vol. 56, No. 2, February 2009, pp. 380–388.